World Journal of Vascular Surgery

Research Article
Published: 16 Mar, 2018

The Role of Biomechanics in the Assessment of Carotid Atherosclerosis Severity: A Numerical Approach

Lina Zouggari[1,2], Benyebka Bou-said[2], Francesco Massi[1], Antonio Culla[1] and Antoine Millon[3]*

[1]Department of Applied Mechanics Engineering DIMA, Sapienza University of Rome, Italy

[2]Laboratory of Contacts and Structure Mechanics LAMCOS, INSA de Lyon, France

[3]Department of Vascular Surgery, University Hospital of Lyon, France

Abstract

Numerical fluid biomechanics has been proved to be an efficient tool for understanding vascular diseases including atherosclerosis. There are many evidences that atherosclerosis plaque formation and rupture are associated with blood flow behavior. In fact, zones of low wall shear stress are vivid areas of proliferation of atherosclerosis, and in particular, in the carotid artery. In this paper a model is presented for investigating how the presence of the plaque influences the distribution of the wall shear stress. In complement to a first approach with rigid walls, an FSI model is developed as well to simulate the coupling between the blood flow and the carotid artery deformation. The results show that the presence of the plaque causes an attenuation of the WSS in the after-plaque region as well as the emergence of recirculation areas.

Keywords: FSI; CFD; Carotid; Atherosclerosis

Introduction

Cardiovascular Accidents (CVAs) cause the death of approximately 6.2 million people per year, according to the World Health Organization [1], and the understanding of how these diseases operate is nowadays a major issue. CVAs are caused by the presence of a clot in the arterial system, 87% of the cases, or by hemorrhages [2]. It is a medical emergency with usually a fatal outcome. One of the major causes of brain CVA's is the carotid atherosclerosis.

Vulnerable plaque is a complex concept [3]. The determination of active plaques remains a clinically relevant topic. As explained by Lafont, the definition of vulnerable plaques includes, in addition to plaque rupture, the plaque erosion, calcification and lack of healing [4]. A variety of parameters can predict a vulnerable plaque [5]. The conventional pathological and imaging markers include intima-media thickness [6], plaque erosion [7,8], thickness of fibrous cap, size of lipidic core and the presence of inflammation along with various biological factors [9,10].

While increasing degree of stenosis can cause the vessel to obstruct, sites with <50% diameter stenosis are the most useful for the detection of vulnerable plaque [11]. The presence of the atherosclerosis plaque, usually in regions of high curvature, led to a widely accepted hypothesis that local loads from hemodynamics play an important role in atherogenesis [12]. It also causes alterations to the systemic behavior such as perturbations to the flow, stress distributions at the wall and particularly the Wall Shear Stress (WSS). In other words, hemodynamics influences the progression of atherosclerosis and its devastating end, i.e. is the plaque rupture.

The effect of the WSS has been investigated by many authors. For many decades, it was believed that atherosclerosis plaques grow in regions where the arterial wall is damaged by high shear caused by blood flow [13,14]. Nevertheless, since the 1960's, authors started to suggest the contrary [15-18]. The development of medical imagery as well as the advancement in the numerical capabilities allowed researchers and clinicians to approach the vascular biomechanics from a different angle [12].

Few studies have established 3D numerical models for diseased Carotid Artery (CA). A study performed by Tang, et al. [19], was the first attempt to investigate the effect of material properties on the stress distributions in an atherosclerosis plaque, using a 3D FSI model. Li, et al. [20] examined the criticality of the fibrous cap thickness by simulating the interaction between blood flow and a stenosed artery under the assumption of Newtonian flow in a simplified geometry. Realizing

OPEN ACCESS

Correspondence:
Lina Zouggari, Department of Applied Mechanics Engineering DIMA, Sapienza University of Rome, Rome, Italy,
E-mail: lina.zouggari@insa-lyon.fr

Received Date: *18 Jan 2018*
Accepted Date: *10 Mar 2018*
Published Date: *16 Mar 2018*

Citation:
Zouggari L, Bou-said B, Massi F, Culla A, Millon A. The Role of Biomechanics in the Assessment of Carotid Atherosclerosis Severity: A Numerical Approach. World J Vasc Surg. 2018; 1(1): 1007.

accurate simulations of hemodynamics consists of the resolution of the Navier-Stokes equations under suitable boundary conditions in an appropriate domain. Recent studies continue exploring the effect of modeling parameters on the results observed in vascular numerical simulations. The inlet and outlet boundary conditions, the viscosity law for the fluid as well as the constitutive law for the arterial wall have been discussed by several authors [21-26]. Concerning the CA, and in order to assess the risk of plaque rupture, early researchers studied mainly 2D models. 3D numerical simulations have been conducted with the assumption of rigid wall simulations [27-29]; lately, new coupling mathematical techniques between the blood flow and the carotid wall have also been investigated [30-33].

In this paper, a finite element model of the CA is developed to simulate the flows and the stresses with and without the presence of the atherosclerosis plaque. First, boundary conditions and fluid flows are investigated on a simplified geometry, deduced from the real geometry of the artery, which offers, a flexibility into the generalization of the results, by accounting for only the main features of real artery geometry. Then, simulations on a patient specific geometry are discussed. The results on the fluid flows will be first presented on a rigid wall model of the artery, and then extended to a full FSI simulation to include the effect of the artery deformation and stress distributions.

Materials and Method

Model geometries

In order to study the effect of stenosis on the circulation within the CA, both simplified and patient-specific geometries have been used. The first one allows for accounting exclusively the main geometrical features common to the human arteries, excluding specific feature of a single patient, but maintaining the main functionally characteristic of the artery. The second one allows for testing and validating the obtained results on a real geometry, recovered by Magnetic Resonance Imagery (MRI) on a specific patient.

The simplified geometry, with the aim of studying the influence of the main geometrical factors, were modeled using CREO, taking into account features of real carotid geometry e.g. curvature, respective diameters of different branches. Both healthy and stenosed arteries with 30% diameter restriction have been modeled (Figures 1a and 1b).

For the specific real geometry, MRI images were obtained from a patient with an atherosclerosis plaque located in the external CA. The geometry of the fluid domain of the carotid bifurcation was segmented and smoothed using SIMPLEWARE and, in order to represent the arterial wall, a layer of 1 mm depth has been added using CATIA.

Mesh

A mesh analysis was carried out to improve the stability of the calculations. Fine hexahedral layers were added at the wall in order to obtain more accurate WSS results. A mean element size of 0.25 mm was used.

Boundary conditions

When modeling flows in vessels of finite dimensions, the definition of the boundary conditions is a delicate step of the model development. For the rigid wall model, the boundary conditions on the fluid have to be defined at both inlet and outlet sections of the model.

In order to approach as much as possible the real behavior of the blood inside the artery, the inlet boundary condition has been directly recovered from 4D MRI images on a patient, which allows for reconstructing the transient variation of the blood velocity. A velocity profile over time was then obtained (Figure 2). A parabolic distribution of the velocity at the inlet boundary was considered, which, in the case of CA, gives the most similar mean WSS with respect to simulations with real patient data, compared to bulk or Womersley profiles [34].

About the outlet boundary condition, different methods were tested to describe the pressure trend at the internal and external Carotid BC's:

- Case 1: Constant pressure of 18 kPa.
- Case 2: Imposed transient pressure, varying periodically with a linear trend from 10 kPa to 18 kPa.
- Case 3: Computed pressure from the 4DMRI results using the Windkessel model, where the numerical values were obtained from the literature [35,36].

The comparison of the tested boundary conditions at the outlet is presented in 5.1.

CFD simulations

The necessity of taking into account the non-Newtonian behavior of blood has been widely discussed in the literature [23]. Nevertheless, a Newtonian behavior of blood has been generally accepted in large arteries [37].

Considering the evolution of viscosity as a function of shear velocity, different models can describe the viscosity of blood (Generalized Newton Models). The parameters experimentally obtained by Cho and Kensey, both Carreau and Casson viscosity models for blood [38], are reported in Table 1 and 2.

As detailed in section 5.2, the Carreau model has been adopted for this study. It is characterized by the presence of

$$\mu = \mu_\infty + (\mu_0 - \mu_\infty)(1 + (\lambda\dot{v})^2)^{\frac{n-1}{2}}$$

μ_∞ : *Viscosity at high shea*

μ_0 : Viscosity at low shear

n : Power index

λ : Time constant

$$\mu = \text{©}\left(\sqrt{\mu_c} + \sqrt{\frac{\tau_c}{\dot{v}}}\right)^2$$

μ_c : *critical stress*

τ_c : *yield stress*

two boards representing low shear viscosity (aggregation of Red Blood Cells (RBCs) and high shear viscosity (RBCs completely disaggregated). Between those two boarders, the blood is a shear thinning fluid. The relation between viscosity and shear velocity is described in the equations above.

The blood was modeled as a laminar incompressible flow with a density of 1,060 kg/m^3 [39]. The Navier Stokes equations are solved using the finite volumes method by FLUENT. The time duration of the simulation was set to 2s allowing the simulation of 3 heart cycles.

Since the flow is considered incompressible, a pressure based

Table 1: Numerical values for the carreau model.

μ_∞ (Pa.s)	μ_0 (Pa.s)	N	λ (s)
0.0035	0.056	0.36	3.3

Table 2: Numerical values for the casson model.

μ_c (Pa.s)	τ_c (Pa)
0.00414	0.0038

Table 3: Mooney rivlin parameters for the arterial tissue.

Parameter	Value (kPa)
C10	50.445
C01	30.491
C20	40
C11	10
C02	120

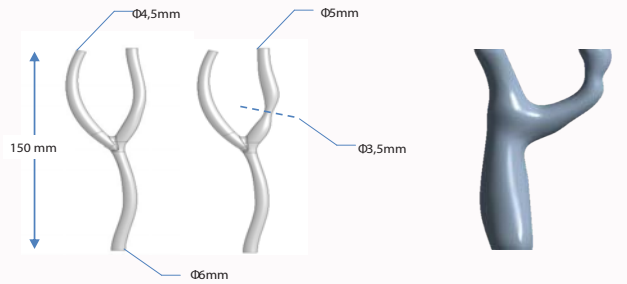

Figure 1: Geometry models: a) Left: simplified geometry with and without plaque. b) Right: Patient specific geometry.

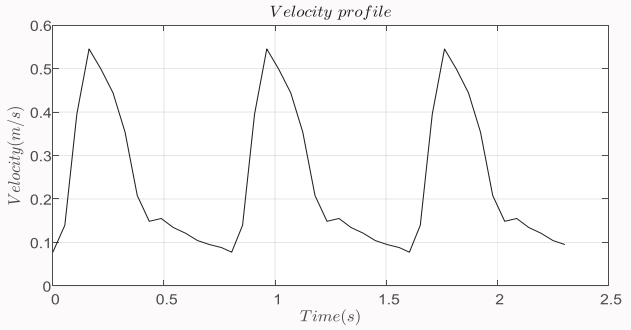

Figure 2: Velocity profile obtained from 4DMRI and prescribed at the inlet (common carotid artery).

solver is used to describe the differential equations. Pressure and viscosity are coupled. In contrast with the SIMPLE algorithm, where a correction is applied to the fluctuations arising from the imposed initial value of the pressure at the first iteration, to insure the continuity of the mass conservation equation, the PISO algorithm uses approximations of higher degrees in the calculus of velocity and pressure.

FSI simulations

After rigid wall simulations for investigating the fluid flow within rigid artery geometry, the artery wall deformations have been introduced into the model to investigate their effect on the flows and stress distributions.

It has been observed that the models describing the arterial wall as a hookean solid are not adequate and cannot describe the blood behavior observed during in vivo measurements [12]. Therefore,

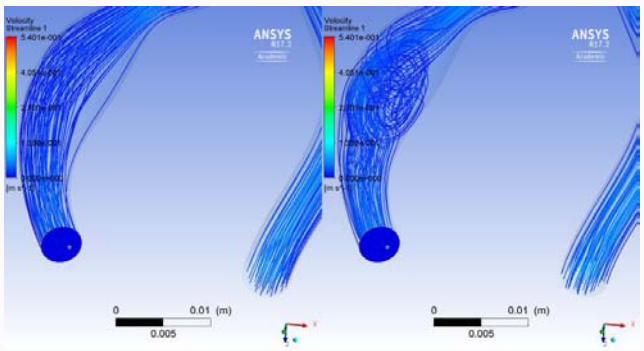

Figure 3: Velocity streamline at early systole left: Simulation results with constant outlet BC, right: Variable pressure at outlet BC.

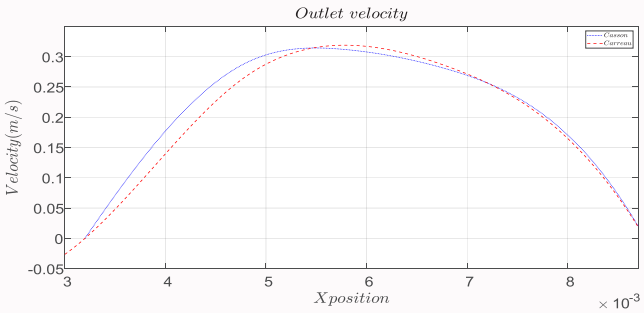

Figure 4: Velocity distribution at ECA. Blue: Carreau Model, Red: Casson model.

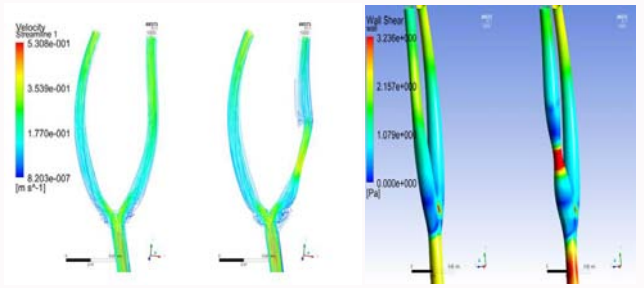

Figure 5: CFD simulation results at t=1.8s in a simplified geometry model, with and without stenosis. Left: 5a) Velocity streamlines at t=1.8s, Right: 5b) WSS distribution.

more representative mechanical models have been used to account for the complexity of the vessel mechanical response [24,40-43], such as large deformations, incompressibility, viscoelasticity.

In the numerical FSI simulations presented in this paper, the mechanical behavior of the structure has been modeled by a hyperelastic 5-parameters Mooney-Rivlin model. The parameters have been obtained from previous experimental tests [19] and fitted by Gao et al. [44], and are reported in Table 3. The arterial tissue is assumed incompressible, i.e. the compressibility coefficient is set to 0.

On the other hand, the plaque region is considered elastic with a Young Modulus set to 0.9 GPa [45]. Computational structure mechanics is performed with the commercial software ASNYS. Large deformations are taken into account.

To solve the FSI problem, the partitioned approach with strong coupling has been adopted. The number of coupling step iterations was set to 20. A convergence analysis has been developed for the

definition of the used mesh, including 6×10^5 structural elements and 1.5×10^6 fluid elements.

The next sections present the results obtained from the developed numerical models to investigate the blood flows and the WSS on the artery with and without the plaque.

Results and Discussion

Both CFD simulations with rigid walls and full FSI simulations with hyperplastic carotid material were performed. A preliminary analysis has been performed for the choice of the viscosity model and the boundary conditions. Then, flow results by the rigid wall model with a simplified geometry are presented and discussed. Finally, full FSI analysis has been performed on a patient specific geometry and compared with rigid wall results. Simulation data were analyzed using CFD post processing software (ANSYS, Inc.). Wall shear stress and blood flows were investigated at different locations of the vasculature with a special focus at the stenosis, after the stenosis and at the bifurcation areas.

Outlet boundary conditions

The first step of the definition of the CFD simulations is the choice of the boundary conditions. The flows from simulations with constant and variable pressure at the outlet are compared. (Figure 3) show noticeable differences, confirming the necessity of using adequate outlet boundary conditions, as discussed abundantly by various authors [22,46]. In fact, the pressure directly affects the behavior of the flow in terms of recirculation and thus WSS.

Lumped Windkessel model has proven to be more accurate for simulating blood flow in the arterial system [22,47]. Nevertheless, it is a time-consuming method especially in the case of coupled approaches. To minimizes the calculation time and preserve the realistic pressure waveform provided by the Windkessel model, the following procedure has been established: in case of available data of the flow in both internal and external carotid arteries from the 4D MRI, the pressure wave form is directly calculated from the available flow rate data using the Windkessel model. In case of unavailability of the measured data, the pressure values are calculated by a preliminary simulation, where the Windkessel model is applied as boundary condition. In both cases, the new pressure profile is used as the transient outlet boundary condition in further simulations.

Comparison of viscosity model

Results from rigid wall simulations in the simplified geometry model, with a variable pressure outlet, have been compared for both Casson and Carreau rheological models. The same boundary conditions and geometry are used, varying the only rheological law introduced in the fluid simulation. (Figure 4) shows the obtained velocity profile at the outlet of the stenosed branch of the carotid bifurcation, internal CA in this case. Slight differences can be observed for both the used models in terms of velocity distribution. Then, for the rest of the simulations, the Carreau model was adopted.

Effect of stenosis on the CFD results

The fluid flow has been simulated in the simplified rigid wall geometry models with and without the presence of the plaque. (Figure 5) shows the velocity streamlines (Figure 5a) and the WSS distribution (Figure 5b) at simulation time 1.8s, corresponding to the systolic peak, with and without plaque. Introducing the stenosis, vortexes are observed after the plaque area, during the late diastole and at the beginning of the systole, where the pressure is at its lowest.

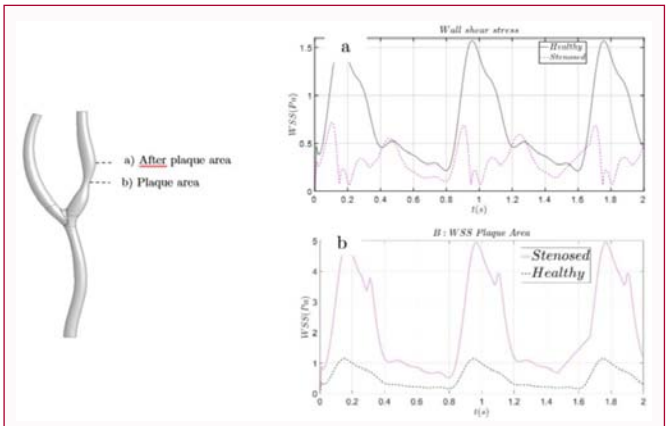

Figure 6: Wall shear stress comparison between healthy and stenosed artery at the plaque and after plaque areas oscillations of the WSS amplitude.

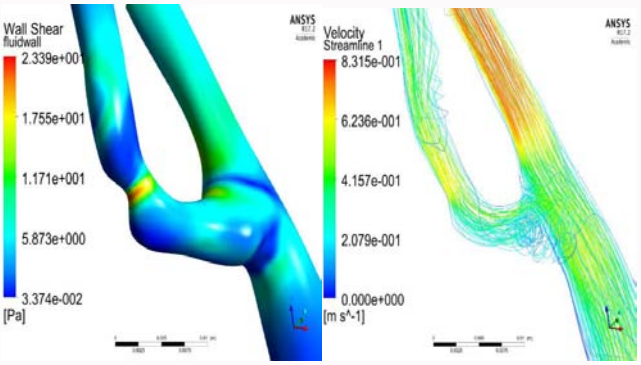

Figure 7: Results of CFD simulation in a patyient-specific geometry: WSS distribution and velocity streamlines at systolic peak.

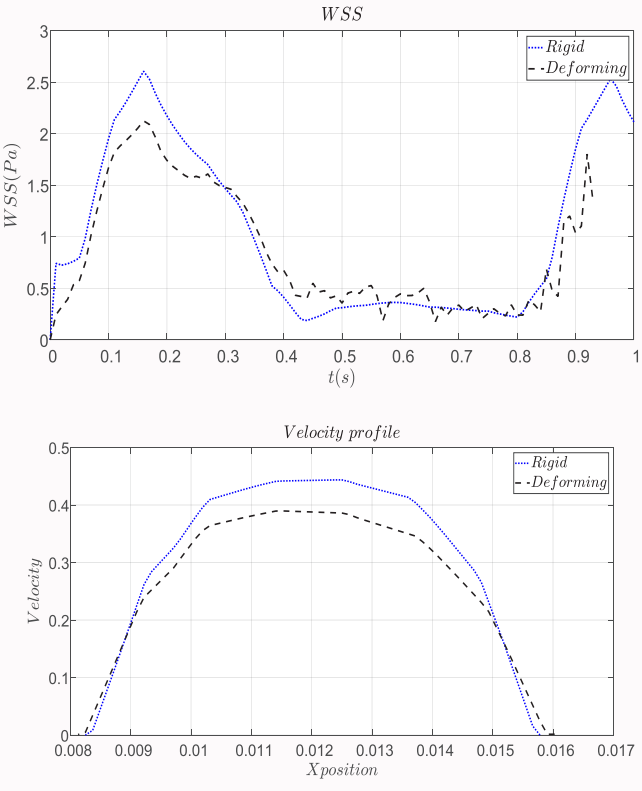

Figure 8: Result comparison between CFD and FSI simulations in an idealized geometry: a) WSS at ICA; b) Velocity profile at ICA outlet (m/s).

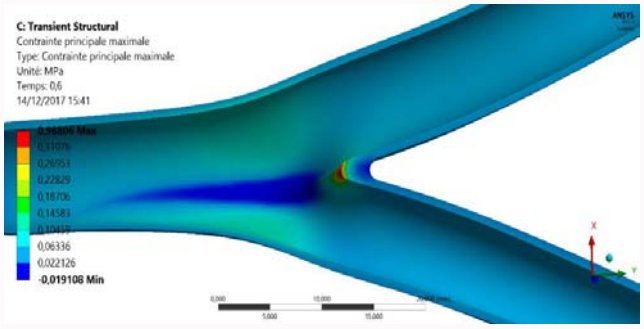

Figure 9: Maximal principal stress at simulation time t=0.6s corresponding to mid diastol in an idealized geometry model.

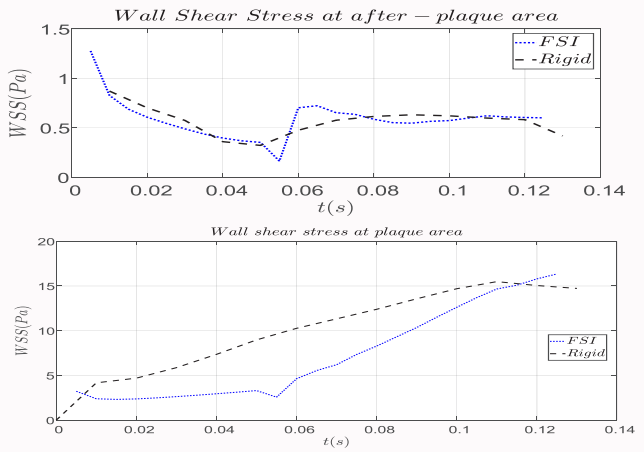

Figure 10: WSS comparison between CFD and FSI simulations: a) After plaque region; b) Plaque region.

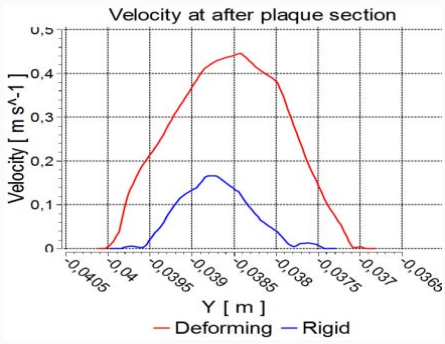

Figure 11: Velocity Profile at stenosed ECA. Comparison between Rigid and Deforming wall patient-specific Simulations at t=0.1.

The WSS shows a completely different distribution as well, with lower values at the after plaque area for the stenosed case.

The mean value of WSS in the CA is reported as 0.850 ± 0.195 (ranging between 0.132-3.464) N/m^2 [48]. Simulation results reported in (Figure 6), and obtained by the simplified model of the healthy artery with rigid walls, are consistent with the literature, falling in the higher range of WSS measured by other authors using imagery techniques [49]. The high values are due to the assumption of rigid wall, while arteries are highly deformable.

The effect of the plaque on the flow behavior is noticeable when comparing the WSS in the case of healthy and stenosed external CA. The comparison in the case of 30% stenosis shows an increase in WSS

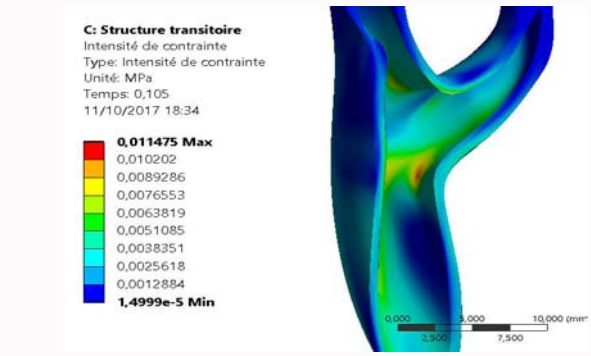

Figure 12: Stress intensity distribution within the arterial wall at the systolic phase.

at the plaque region by 5 times (Figure 6b). The results also indicate a strong decrease as well of the maximum WSS observed after the plaque region as well as the emergence of further oscillations of the WSS amplitude (Figure 6a).

The results also highly depend on the geometry, which confirms the necessity of patient specific simulations to obtain more accurate results. Running CFD simulations on patient specific geometry resulted in the same general flow behavior observed in the simplified geometry cases. LWSS and recirculation have also been observed in the after plaque and the bifurcation area as in the previous case scenario. The WSS values ranged from 0.03 Pa to 24 Pa in the systolic phase (Figure 7). As well, a decrease of the WSS at the after plaque zone is observed with the patient geometry.

FSI Results

FSI simulations were first run on simplified geometries to compare the results with the rigid wall simulations on a generic geometry. The comparison between rigid wall and coupled simulations shows the conservation of the general distribution form of the WSS in the branches of the carotid (Figures 8-10), with a decrease in the mean value of the velocity, due to the deformation of the wall and thus the decrease of the shear rate. This observation is very clear at the bifurcation area where the extension of the recirculation zones is notable. The fluctuations in the values of the calculated velocity, as well as of the WSS (Figure 8a), during diastole might be a consequence of the rigid clamping conditions at the boundaries of the structure, causing reflection waves.

The velocity in the stenosed branch, as shown in (Figure 11), is higher than in the case of rigid wall simulation, due to the extensibility of the wall. Relatively more blood, at the considered time, is flowing to the brain. The wall shear stress is in the same range as for the CFD simulations with rigid walls. FSI, on the other side, allows for obtaining the stress distribution within the arterial wall as shown in (Figure 12).

Preliminary FSI simulations in simplified geometries, but a tangible difference is observed at the plaque area. Generally, into the literature, 4D MRI derived WSS is lower than CFD derived WSS [49-53], with highest difference in high wall shear stress zones, which is compatible with the difference observed between FSI and CFD in our model. Nevertheless, the study conducted by Boussel, et al. leads to opposite conclusions with a WSS 8 times higher than CFD results [54]. As discussed by Jeremy Sjar and Kevin Ho-Shon, the high WSS observed by Boussel might be due to the methodology used to estimate the velocity in voxels that were partially outside the Lumen

[55].

The disparity between CFD and FSI, or MRI results is mainly due to the partial volume effects that lead in significant volume change [55]. Nevertheless, numerical simulations have higher resolution at the wall, compared to MRI resolution. With the augmentation of velocity due to the presence of the plaque, the use of MRI techniques becomes impractical due to the thinning of the boundary wall layer.

Studies on fluid dynamics show that the flow and the WSS are disturbed near to the carotid bifurcation, which may cause endothelial dysfunction. LWSS has a significant role in inducing arterial damage and plaque instability due to the increase of residual time and therefore platelets and macrophage probability of adhesion to the arterial wall [56]. Moreover, it seems that chronic exposure to high WSS causes an atheroprotective phenotype [57] and, probably, a remodeling phenomenon. Investigations should be carried out to confirm this hypothesis.

Although CFD is the most used method, the presented results showed that it tends to overestimate the WSS, especially in high shear rate regions. The FSI simulations, on the other side, give a more realistic appreciation of the shear rate. The accuracy of those methods is still unknown, and depends highly on the boundary conditions. With the promising advancement in MRI resolution and the decrease of scanning time, the potential of improving both the boundary conditions and having a solid model comparison is increasing.

Conclusion

A CFD and FSI models of the CA has been presented in this paper using simplified and patient specific geometries. Variation of hemodynamic simulations parameters, i.e. rheological model and outlet boundary conditions, has been investigated in order to verify their accuracy.

The comparison between healthy and stenosed arteries showed a diversity of flow disruptions near the stenosis area resulting in a higher shear stress in the plaque zone and lower shear stress in the after-plaque zone. This result was observed both in the generic simplified geometry and in the patient specific geometry.

The plaque rupture depends among others on the local WSS and the local strength of the tissue. On one hand LWSS zones are areas of vivid proliferation of atherosclerosis plaques, on the other hand the LWSS can promote inflammations and cause plaque instability too.

A considerable difference between the FSI and CFD results has been obtained. The WSS is undeniably higher for the rigid wall simulation. The difference in the WSS results between FSI and CFD simulations support the choice of the coupled method.

There were several limitations in this study. Time consuming calculations reduces the possibility to run multiple patient specific simulations. Nevertheless, the aim of this work was to develop a numerical model accounting for patient specific data in order to investigate the mechanical parameters contributing to the development and rupture of atherosclerosis plaques within the CA. The material properties used for the plaque, corresponding to a purely elastic material, as well as the assumption of uniform wall thickness might influence the observed results too. High resolution imagery, along with mechanical characterization of the various components of calcified CA, will allow for investigating accurately the stress distributions in the fibrous cap.

Acknowledgement

We gratefully thank Pr. LoicBoussel and Dr. Monica Sigovan from the department of radiology of Croix Rousse Hospital of Lyon for providing us the necessary Data to this work.

References

1. Department of Health Statistics and Informatics. World Health Organization Geneva, Causes of death 2008: data sources and methods. April. 2011.
2. Writing Group Members, Mozaffarian D, Benjamin EJ, Go AS, Arnett DK, Blaha MJ, et al. Heart disease and stroke statistics-2016 update: A Report from the American Heart Association. Circulation. 2016;133(4):e38-360.
3. Tuenter A, Selwaness M, Lorza AA, Schuurbiers JCH, Speelman L, Cibis M, et al. High shear stress relates to intraplaque haemorrhage in asymptomatic carotid plaques. Atherosclerosis. 2016;251:348-54.
4. Lafont A. Basic aspects of plaque vulnerability. Heart. 2003;89(10):1262-7.
5. Nighoghossian N, Derex L, Douek P. The vulnerable carotid artery plaque: current imaging methods and new perspectives. Stroke. 2005;36(12):2764-72.
6. Hollander M, Hak AE, Koudstaal PJ, Bots ML, Grobbee DE, Hofman A, et al. Comparison between measures of atherosclerosis and risk of stroke: The Rotterdam Study. Stroke. 2003;34(10):2367-72.
7. Farb A, Burke AP, Tang AL, Liang TY, Mannan P, Smialek J, et al. Coronary plaque erosion without rupture into a lipid core. A frequent cause of coronary thrombosis in sudden coronary death. Circulation. 1996;93(7):1354-63.
8. Meairs S, Timpe L, Beyer J, Hennerici M. Acute aphasia and hemiplegia during karate training. Lancet. 2000;356(9223):40.
9. Naghavi M, Libby P, Falk E, Casscells SW, Litovsky S, Rumberger J, et al. From vulnerable plaque to vulnerable patient. Circulation. 2003;108(14):1664-72.
10. Faxon DP, Creager MA, Smith SC Jr, Pasternak RC, Olin JW, Bettmann MA, et al. Atherosclerotic vascular disease conference: executive summary: atherosclerotic vascular disease conference proceeding for healthcare professionals from a special writing group of the american heart association. Circulation. 2004;109(21):2595-604.
11. Virmani R, Burke AP, Farb A, Kolodgie FD. Pathology of the vulnerable plaque. J Am Coll Cardiol. 2006;47(8 Suppl):C13-8.
12. Taylor CA, Humphrey JD. Open problems in computational vascular biomechanics: hemodynamics and arterial wall mechanics. Comput Methods Appl Mech Eng. 2009;198(45-46):3514-23.
13. Duguid Jb, Robertson Wb. Mechanical factors in atherosclerosis. Lancet. 1957;272(6981):1205-9.
14. McDonald DA. The Velocity Profiles in Pulsatile Blood Flow. Presented at the Flow properties of blood and other biological systems: proceedings of an informal discussion convened jointly by the Faraday Society Colloid and Biophysics Committee and the British Society of Rheology, held at the University Laboratory of Physiology, Oxford, 23 and 24 September, 1959.
15. Porter R, Knight J, editors. Ciba Foundation Symposium 12 - Atherogenesis: Initiating Factors. John Wiley & Sons, Ltd; 1973.
16. Gessner FB. Brief reviews: Hemodynamic theories of atherogenesis. Circ Res. 1973;33:259-66.
17. Malek AM, Alper SL, Izumo S. Hemodynamic shear stress and its role in atherosclerosis. JAMA. 1999;282(21):2035-42.
18. Caro CG. Discovery of the role of wall shear in atherosclerosis. Arterioscler Thromb Vasc Biol. 2009;29(2):158-61.
19. Tang D, Yang C, Zheng J, Woodard PK, Sicard GA, Saffitz JE, et al. 3D

MRI-based multicomponent FSI models for atherosclerotic plaques. Ann Biomed Eng. 2004;32(7):947-60.

20. Li ZY, Howarth SP, Tang T, Gillard JH. How critical is fibrous cap thickness to carotid plaque stability? a flow-plaque interaction model. Stroke. 2006;37(5):1195-9.

21. Holzapfel GA, Mulvihill JJ, Cunnane EM, Walsh MT. Computational approaches for analyzing the mechanics of atherosclerotic plaques: a review. J Biomech. 2014;47(4):859-69.

22. Vignon-Clementel IE, Figueroa CA, Jansen KE, Taylor CA. Outflow boundary conditions for 3D simulations of non-periodic blood flow and pressure fields in deformable arteries. Comput Methods Biomech Biomed Engin. 2010;13(5):625-40.

23. Amblard A, Berre HW, Bou-Saïd B, Brunet M. Analysis of type I endoleaks in a stented abdominal aortic aneurysm. Med Eng Phys. 2009;31(1):27-33.

24. Avril S. Hyperelasticity of soft tissues and related inverse problems. Mater Parameter Identif Inverse Probl Soft Tissue Biomech. 2016;573:37-66.

25. Pierre B, Stéphane A, Susan L, Michael S. Mechanical identification of hyperelastic anisotropic properties of mouse carotid arteries. New York: Conf Proc Soc Exp Mech Ser Springer; 2011. p. 11-7.

26. Teng Z, Canton G, Yuan C, Ferguson M, Yang C, Huang X, et al. 3D critical plaque wall stress is a better predictor of carotid plaque rupture sites than flow shear stress: an in vivo MRI-based 3D FSI study. J Biomech Eng. 2010;132(3):031007.

27. Campbell IC, Timmins LH, Giddens DP, Virmani R, Veneziani A, Rab ST, et al. Computational fluid dynamics simulations of hemodynamics in plaque erosion. Cardiovasc Eng Technol. 2013;4(4).

28. Schirmer CM, Malek AM. Computational fluid dynamic characterization of carotid bifurcation stenosis in patient-based geometries. Brain Behav. 2012;2(1):42-52.

29. Conti M, Long C, Marconi M, Berchiolli R, Bazilevs Y, Reali A. Carotid artery hemodynamics before and after stenting: A patient specific CFD study. Comput Fluids. 2016;141:62-74.

30. Gao H, Long Q, Graves M, Gillard JH, Li ZY. Carotid arterial plaque stress analysis using fluid-structure interactive simulation based on in-vivo magnetic resonance images of four patients. J Biomech. 2009;42(10):1416-23.

31. Cilla M, Borras I, Pena E, Martinez M, Malve M. A parametric model for analysing atherosclerotic arteries: On the FSI coupling. Int Commun Heat Mass Transf. 2015;67:29-38.

32. Langer U, Yang H. Partitioned solution algorithms for fluid–structure interaction problems with hyperelastic models. J Comput Appl Math. 2015;276:47-61.

33. Langer U, Yang H. Numerical simulation of fluid–structure interaction problems with hyperelastic models: A monolithic approach. Math Comput Simul. 2018;145:186-208.

34. Campbell IC, Ries J, Dhawan SS, Quyyumi AA, Taylor WR, Oshinski JN. Effect of inlet velocity profiles on patient-specific computational fluid dynamics simulations of the carotid bifurcation. J Biomech Eng. 2012;134(5):051001.

35. Holzapfel G, Kuhl E, editors. Computer models in biomechanics: from nano to macro. Dordrecht, Netherlands: Springer; 2011.

36. Figueroa CA, Coogan JS, Humphrey JD. Hemodynamic alterations associated with coronary and cerebral arterial remodeling following a surgically-induced aortic coarctation. In: Holzapfel G, Kuhl E, editors. Computer Models in Biomechanics. Dordrecht, Netherlands: Springer; 2013. p. 203-16.

37. Jaffrin MY, Goubel F. Biomécanique des fluides et des tissus. Masson. 1998.

38. Cho YI, Kensey KR. Effects of the non-Newtonian viscosity of blood on flows in a diseased arterial vessel. Part 1: Steady flows. Biorheology 1991;28(3-4):241-62.

39. Cutnell JD, Johnson KW. Physics. 4th ed. New York: Wiley; 1997.

40. Ogden RW. Large deformation isotropic elasticity: On the correlation of theory and experiment for compressible rubberlike solids. Proc R Soc Math Phys Eng Sci. 1972;328(1567):567-83.

41. Holzapfel GA, Gasser TC, Ogden RW. A new constitutive framework for arterial wall mechanics and a comparative study of material models. J Elast Phy Sci Soli. 2000;61(1-3):1-48.

42. Cheng T, Dai C, Gan RZ. Viscoelastic properties of human tympanic membrane. Ann Biomed Eng. 2007;35(2):305-14.

43. Kaazempur-Mofrad M, Younis H, Patel S, Isasi A, Chung C, Chan R, et al. Cyclic strain in human carotid bifurcation and its potential correlation to atherogenesis: Idealized and anatomically-realistic models. J Eng Math. 2003;47(3-4):299-314.

44. Gao H, Long Q. Effects of varied lipid core volume and fibrous cap thickness on stress distribution in carotid arterial plaques. J Biomech. 2008;41(14):3053-9.

45. Mouktadiri G. Angiovision-Pose d'endoprothèse aortique par angionavigation augmentée. Villeurbanne: INSA-Lyon; 2013; 2013.

46. Figueroa CA, Humphrey JD. Pressure wave propagation in full-body arterial models: A gateway to exploring aging and hypertension. Procedia IUTAM. 2014;10:382-95.

47. Du T, Hu D, Cai D. Outflow boundary conditions for blood flow in arterial trees. PLoS One. 2015;10(5):e0128597.

48. Sui B, Gao P, Lin Y, Gao B, Liu L, An J. Assessment of wall shear stress in the common carotid artery of healthy subjects using 3.0-tesla magnetic resonance. Acta Radiol. 2008;49(4):442-9.

49. Cibis M, Potters WV, Selwaness M, Gijsen FJ, Franco OH, Arias Lorza AM, et al. Relation between wall shear stress and carotid artery wall thickening MRI versus CFD. J Biomech. 2016;49(5):735-41.

50. Van Ooij P, Potters WV, Guédon A, Schneiders JJ, Marquering HA, Majoie CB, et al. Wall shear stress estimated with phase contrast MRI in an in vitro and in vivo intracranial aneurysm. J Magn Reson Imaging 2013;38(4):876-84.

51. Isoda H, Ohkura Y, Kosugi T, Hirano M, Alley MT, Bammer R, et al. Comparison of hemodynamics of intracranial aneurysms between MR fluid dynamics using 3D cine phase-contrast MRI and MR-based computational fluid dynamics. Neuroradiology. 2010;52(10):913-20.

52. Kohler U, Marshall I, Robertson MB, Long Q, Xu XY, Hoskins PR. MRI measurement of wall shear stress vectors in bifurcation models and comparison with CFD predictions. J Magn Reson Imaging. 2001;14(5):563-73.

53. Papathanasopoulou P, Zhao S, Kohler U, Robertson MB, Long Q, Hoskins P, et al. MRI measurement of time-resolved wall shear stress vectors in a carotid bifurcation model, and comparison with CFD predictions. J Magn Reson Imaging. 2003;17(2):153-62.

54. Boussel L, Rayz V, Martin A, Acevedo-Bolton G, Lawton MT, Higashida R, et al. Phase-contrast magnetic resonance imaging measurements in intracranial aneurysms in vivo of flow patterns, velocity fields, and wall shear stress: Comparison with computational fluid dynamics. Magn Reson Med. 2009;61(2):409-17.

55. Szajer J, Ho-Shon K. A comparison of 4D flow MRI-derived wall shear stress with computational fluid dynamics methods for intracranial aneurysms and carotid bifurcations - A review. Magn Reson Imaging. 2017;48:62-69.

56. Resnick N, Collins T, Atkinson W, Bonthron DT, Dewey CF, Gimbrone MA. Platelet-derived growth factor B chain promoter contains a cis-

acting fluid shear-stress-responsive element. Proc Natl Acad Sci USA. 1993;90(10):4591-5.

57. Traub O, Berk BC. Laminar shear stress: mechanisms by which endothelial cells transduce an atheroprotective force. Arter Thromb Vasc Biol. 1998;18(5):677-85.